

Supporting Information

Inclusion of 4-pyrrolidinopyridine derivatives in a symmetrical $\alpha,\alpha',\delta,\delta'$ -tetramethyl-cucurbit[6]uril and a Ba²⁺-driven pseudorotaxane with characteristic UV absorption changes

Bo Yang,^a Xin Xiao,^{*a} Yun-Qian Zhang,^a Qian-Jiang Zhu,^a Sai-Feng Xue,^a Zhu Tao,^a and Gang Wei^{*b}

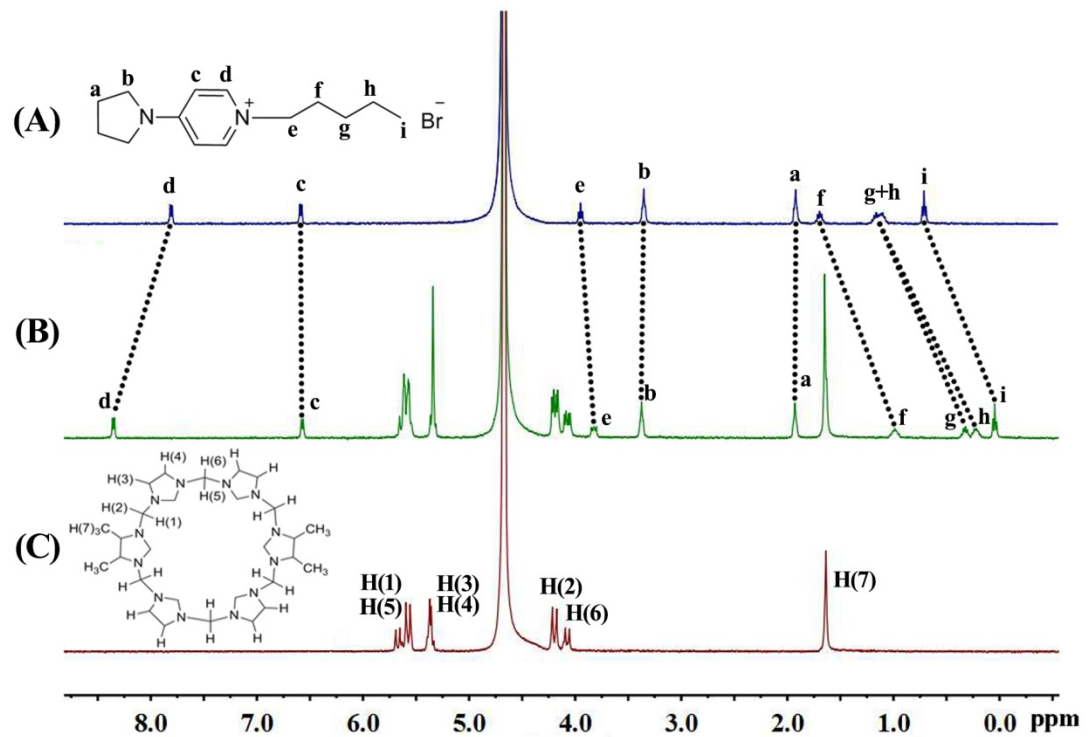


Fig. S1 Interaction of g2 and TMeQ[6]: ^1H NMR spectra (400 MHz, D_2O) of (A) g2 (ca. 2 mM) in the absence TMeQ[6], (B) in the presence of 1.19 equiv of TMeQ[6], and (C) neat TMeQ[6].

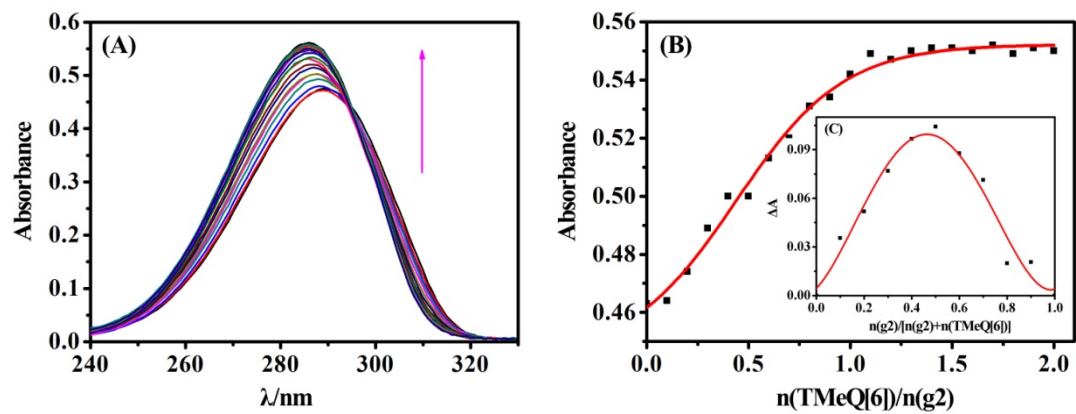


Fig. S2 Interaction of g2 and TMeQ[6]: (A) absorption spectra of g2 (20 μM) in aqueous solution at different TMeQ[6] concentrations, (B) concentrations and the corresponding A vs $N_{\text{TMeQ}[6]}/N_{\text{g}2}$ curve and (C) concentrations and the corresponding ΔA vs $N_{\text{g}2}/(N_{\text{TMeQ}[6]}+N_{\text{g}2})$ curve (inset).

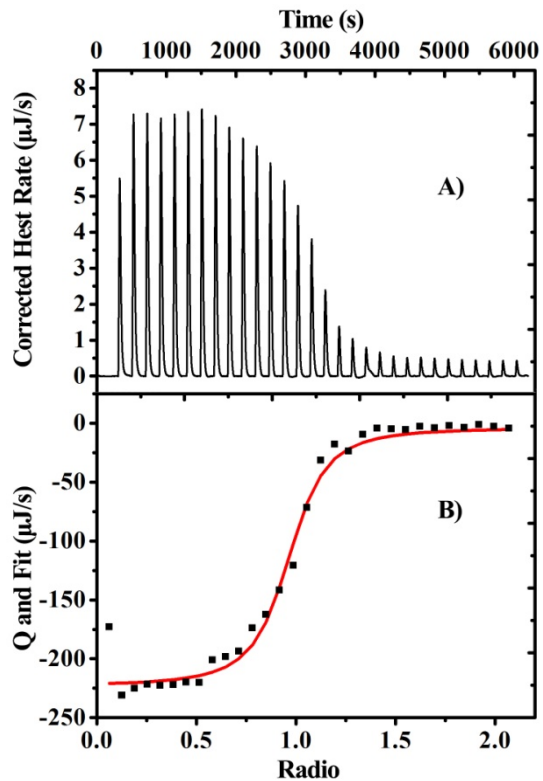


Fig. S3 Isothermal titration calorimetry profiles of TMeQ[6] with g2 in aqueous solution at 298.15 K. A) Nano ITC data for 30 sequential injections (each of 6 mL) of g2 solution (1.0 mM) into TMeQ[6] solution (0.1 mM). B) Apparent reaction heat obtained from integration of the calorimetric traces.

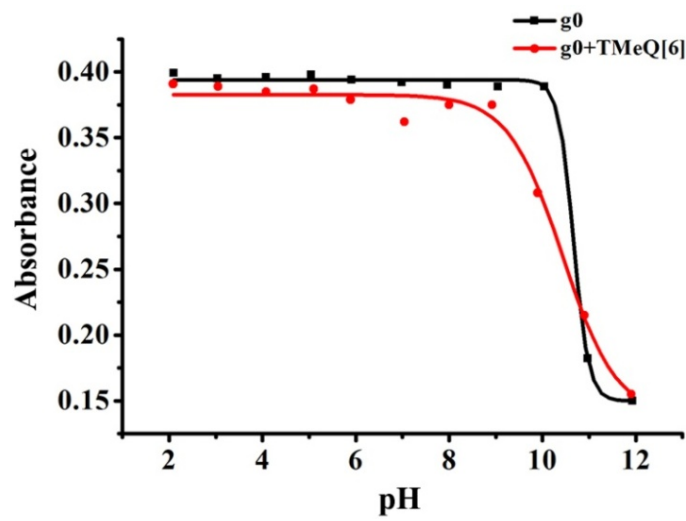


Fig. S4 UV pH titrations of g0 (■) (282nm) and TMeQ[6]·g0 complexes (●) (282nm)

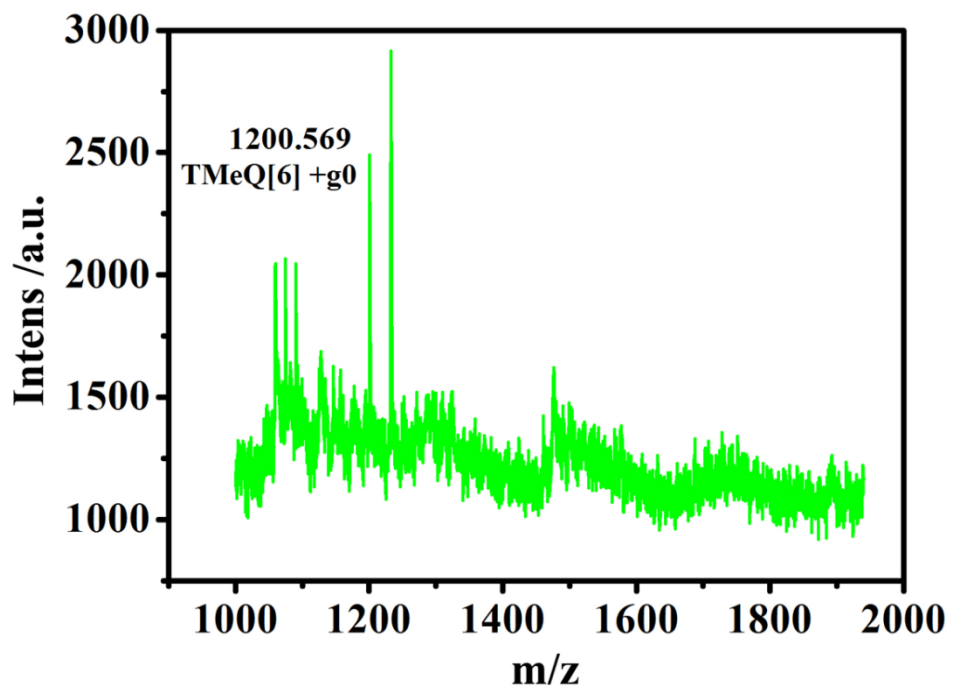


Fig. S5 The MALDI-TOF mass spectrum for TMeQ[6]·g0.

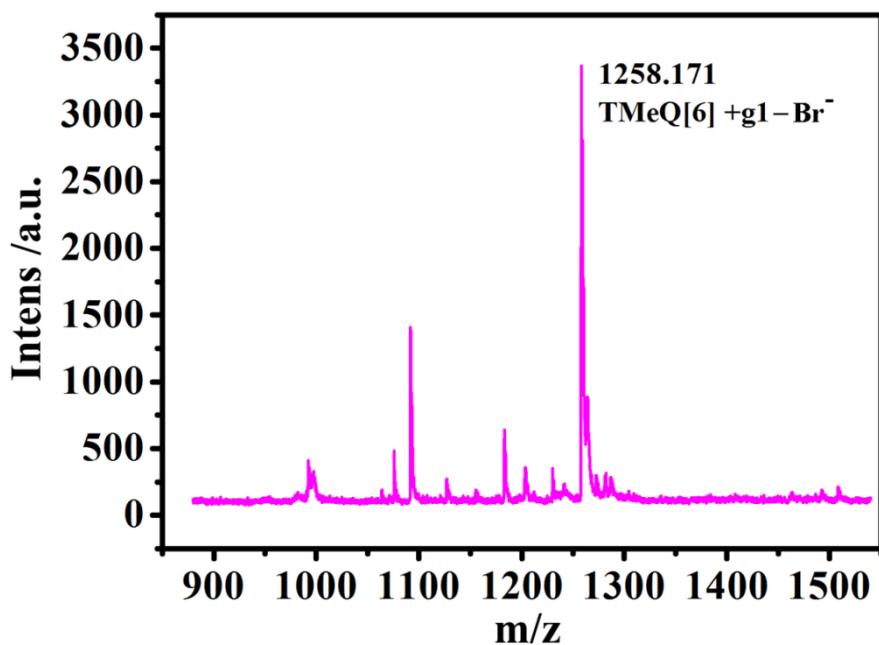


Fig. S6 The MALDI-TOF mass spectrum for TMeQ[6]·g1.

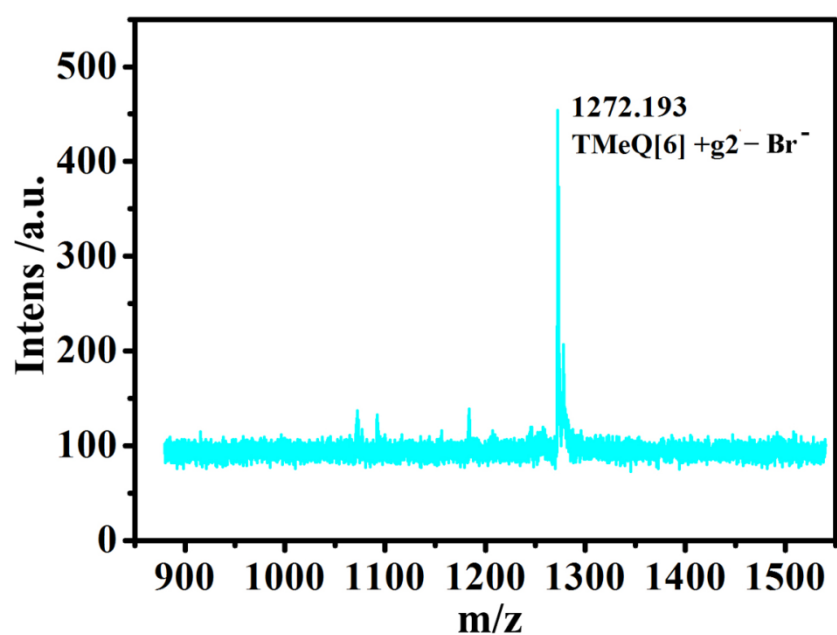


Fig. S7 The MALDI-TOF mass spectrum for TMeQ[6]·g2.

Table S1 Microcalorimetric titration data for TMeQ[6] with g2 in aqueous solution at 298.15 K.

Complex	<i>n</i>	<i>Ka</i> (M ⁻¹)	<i>ΔH</i> (kJ mol ⁻¹)	<i>TΔS</i> (kJ mol ⁻¹)
g2-TMeQ[6]	0.94±0.02	(1.08±0.32) × 10 ⁶	-36.60±0.87	-2.16

